AIAA JOURNAL
Vol. 36, No. 7, July 1998

Tomographic Analysis of Unsteady, Reacting Flows: Numerical Investigation

Erik D. Torniainen,* Alexander K. Hinz,† and Frederick C. Gouldin‡
Cornell University, Ithaca, New York 14853

The implementation of a new tomographic inversion method as a combustion diagnostic tool for the study of unsteady, reacting flows is evaluated using numerical experiments to reconstruct two-dimensional fuel concentration distributions obtained from a numerical simulation of a turbulent reacting square jet. Reconstructions of nonaxisymmetric fuel concentration distributions are performed at various downstream locations from the jet exit using only a few line integrals made along multiple offsets and viewing angles. The new inversion method expresses the concentration distributions to be reconstructed as a weighted sum of Karhunen–Loève eigenfunctions, produced by the Karhunen–Loève procedure. These Karhunen–Loève eigenfunctions and their associated time coefficients are mathematically constructed to form an optimal representation of the concentration distributions in the square jet and systematically quantify their spatial and temporal downstream evolution. Near the exit of the jet, only one eigenfunction is needed, and farther downstream more eigenfunctions (up to 24) are needed to capture the significant features in the concentration distributions. Ultimately, accurate reconstructions of the fuel concentration distributions at downstream locations away from the jet exit are obtained using only 28 line integrals. The effect of the number of eigenfunctions used in the reconstruction and the measurement configuration on the reconstruction accuracy is examined.

Nomenclature

A	= matrix of time coefficients
a_i	= associated time coefficient determined via Karhunen–Loève procedure
C	= matrix of concentration distributions
c	= concentration distribution
$\hat{c}$	= best representation of concentration distribution
c_{recons}	= reconstructed concentration distribution
D	= two-time correlation matrix
dx	= grid spacing of numerical output
E_M	= amount of information contained in M eigenfunctions
G	= integration matrix
I	= intensity of laser at detector
I_0	= intensity of laser at source
k	= discrete time indicator
k_v	= absorption coefficient distribution
M	= number of eigenfunctions used in the reconstruction
N_B	= number of basis functions used to perform reconstruction
N_L	= number of line integrals used to perform reconstruction
N_M	= number of Karhunen–Loève eigenfunctions
N_p	= total number of spatial points
N_t	= total number of time realizations
N_x	= number of points in x direction
N_y	= number of points in y direction
P^ϕ	= eigenfunction projection matrix
$\boldsymbol{p}^c$	= vector of line integrals through a concentration distribution
s	= coordinate representing the location of line-of-sight measurement at a particular viewing angle
t	= coordinate in the direction of line-of-sight measurement
x, y	= Cartesian coordinates
α	= vector of basis function coefficients
α_i	= ith basis function coefficient
θ	= angle between x axis and s axis
$\kappa(P^\phi)$	= condition number of eigenfunction projection matrix
Λ	= eigenvalue matrix
λ_i	= ith eigenvalue
$\bar{\lambda}_i$	= normalized ith eigenvalue
σ_i	= ith singular value of the eigenfunction projection matrix
Φ	= Karhunen–Loève eigenfunction matrix
ϕ_i	= ith Karhunen–Loève eigenfunction

Presented as Paper 97-0257 at the AIAA 35th Aerospace Sciences Meeting, Reno, NV, Jan. 6–9, 1997; received March 24, 1997; revision received Feb. 12, 1998; accepted for publication Feb. 16, 1998.

*Graduate Student, Sibley School of Mechanical and Aerospace Engineering, 112 Upson Hall.

†Graduate Student, Sibley School of Mechanical and Aerospace Engineering; currently Technical Staff, Darmstadt University of Technology, Energie und Kraftwerkstechnik, Darmstadt 64287, Germany.

‡Professor, Sibley School of Mechanical and Aerospace Engineering, 112 Upson Hall. Associate Fellow AIAA.

I. Introduction

THE motivation for the work presented is the application of a new tomographic inversion method to the study of unsteady reacting flows. The potential of this new inversion method, tomographic reconstruction via a Karhunen–Loève basis (TRKB method), to operate effectively as a combustion diagnostic tool is evaluated using numerical experiments performed on data obtained from a numerical simulation of a turbulent, reacting square jet. These numerical experiments simulate the implementation of the TRKB method on an unsteady, reacting flow and provide information as to the applicability and performance of the TRKB method in combustion applications.

The TRKB method takes advantage of all available a priori information regarding the system under investigation and accurately reconstructs nonaxisymmetric, two-dimensional scalar distributions using only a few well-configured, line-of-sight measurements. The novel feature of the TRKB method is the expansion of the distribution to be reconstructed as a weighted sum of Karhunen–Loève (K–L) eigenfunctions formed from a training set, containing the a priori information, using the K–L procedure.[1,2] A priori information is knowledge regarding the characteristics of the distributions to be reconstructed, such as the physical extent, nonnegativity, or shape of the distributions. The K–L procedure is a general mathematical analysis tool that constructs the K–L eigenfunctions in an optimal manner in the sense that the K–L eigenfunctions more accurately represent distributions in the training set using fewer terms than any other basis function. In the TRKB method, the a priori information is contained in a training set as a set of distributions that are representative of the distributions to be reconstructed. Because the K–L eigenfunctions are optimal, only a few eigenfunctions are typically needed to capture the prominent features of the distributions in the training set. Consequently, only a few line-of-sight measurements are needed to determine the contribution

of each eigenfunction in a reconstruction. In addition, note that the K–L eigenfunctions can represent all types of distributions, even those containing discontinuities.[3–5]

Previous work has shown that temperature and concentration distributions can be retrieved in a nonreacting, steady flow with relatively few measurements provided that an appropriate training set is available.[3–6] An extensive amount of a priori information is required to construct the distributions in the training set, and this information can be assembled in a number of ways, including numerical simulation (as in the present case) and in situ probe sampling.[4,5] Previous studies have used training sets containing relatively few members, which were rather arbitrary in the sense that they were produced intentionally to test the TRKB method.[3–6]

Many combustion systems are unsteady (turbulent) and can exhibit many degrees of freedom. In this paper, we evaluate the construction of the training set and the performance of the TRKB method given data representative of combustion systems. We utilize the numerical simulation of a forced, turbulent reactive square jet produced by Grinstein and Kailasanath[7] of the Naval Research Laboratory. This reacting flow, described in detail in the next section, is a turbulent reacting square jet of N_2 and H_2 issuing (with a periodic forcing) into a quiescent background of N_2 and O_2 at a Reynolds number greater than 8.5×10^4 based on the equivalent jet diameter. The training set contains fuel (H_2) concentration distributions produced by the square jet simulation at a given downstream location for a series of time realizations. Unlike previous work with the TRKB method, the distributions in the training set are taken from an unsteady, reacting flow not intentionally produced to evaluate the TRKB method. The use of this square jet simulation, characteristic of an unsteady combustion situation, allows the TRKB method to be tested in the most realistic situation to date.

Previous work has been performed by a number of investigators to study the application of tomographic inversion methods to combustion systems.[8–12] The difference distinguishing the TRKB method from these previous works is the focus on the reconstruction of nonaxisymmetric, two-dimensional distributions using as few measurements as possible (note that the objective of Ref. 12 was also few measurements). The need for only a small number of measurements allows the TRKB method to be implemented in situations where other tomographic methods requiring many line-of-sight measurements, i.e., Fourier methods,[13,14] may not be feasible.

The practical implementation of the TRKB method requires that rapid line-of-sight absorption measurements be made at multiple viewing angles. Work is currently in progress at Cornell University to develop a measurement system that can be used to make up to 720 absorption measurements distributed over six viewing angles as needed for reconstructions via the TRKB method. An array of high-speed InAs infrared detectors in conjunction with two tunable infrared color center lasers is planned to make these measurements. As an initial step, concentration distributions will be reconstructed in an unsteady flow at a known temperature. The training set needed for the TRKB method will be obtained by experiment, possibly using another tomographic inversion method, Finite Domain Direct Inversion (FDDI),[12] or by computer simulation. It is planned that eventually time-resolved temperature and concentration distributions will be reconstructed from measurements made using two color-center lasers.

The reconstruction of concentration distributions from the square jet simulation using the TRKB method is decomposed into two steps. The first step, the representation step, is the K–L analysis of a set of concentration distributions for a series of time intervals at a given downstream location. It is important to establish the suitability of a subset of K–L eigenfunctions, containing only a small number of eigenfunctions, to effectively represent the distributions at a given downstream location and capture the significant features. The eigenfunctions thus determined are used as basis functions in the second step, the inversion step. The inversion step is the reconstruction of a concentration distribution at a given downstream location given a set of line integrals.

II. Turbulent Reacting Square Jet

The data used in this paper were produced from a numerical simulation of a turbulent reacting square jet performed by Grinstein and Kailasanath[7] at the Naval Research Laboratory. An initially laminar jet of the fuel H_2 diluted in N_2 issues into a quiescent background of O_2 diluted in N_2. The jet exit velocity is 200 m/s with a Mach number equal to 0.3. The background gases are at 1 atm and 1400 K to ensure autoignition of the jet. The jet has a Reynolds number $>8.5 \times 10^4$ based on the equivalent jet diameter D_e. The computations were performed for 80 time steps on a grid containing $80 \times 80 \times 120$ grid points and output onto a grid containing $60 \times 60 \times 120$ grid points. The individual cell spacing dx of the output grid is equal to 0.015 cm, and the equivalent jet diameter D_e is equal to $22.56dx$. The exit jet velocity is forced sinusoidally through velocity fluctuations at an rms level of 2.5% of the jet exit velocity over a period of 10 time steps. Ultimately, for our investigation we examined the fuel (H_2) concentration distributions at downstream locations indicated by $5dx$, $15dx$, $25dx$, ..., $115dx$. Figure 1 shows the jet under investigation. Further details regarding the square jet simulation can be obtained in Ref. 7.

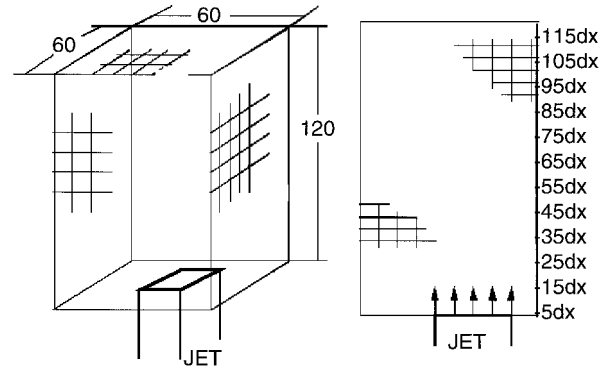

Fig. 1 Domain of the square jet simulation extends ± $3D_e$ from the jet axis in the cross-stream direction and $5.3D_e$ downstream from the jet exit; downstream locations of interest are $5dx$, $15dx$, etc., indicating the distance from the jet exit.

III. TRKB Method

A. Background: Tomographic Inversion

The TRKB method[3] is a tomographic inversion method developed to reconstruct an unknown, two-dimensional distribution from a small number of well-configured, line-of-sight measurements. The central mathematical problem in the general field of tomographic inversion is the reconstruction of an unknown distribution from line-of-sight measurements obtained through the absorption, emission, or reflectance of a probe, e.g., laser beam and x rays.[13] A line-of-sight measurement along an offset s and angle θ is defined mathematically by the line integral

$$p^c(s,\theta) = \int_{-\infty}^{+\infty} c(s\cos\theta - t\sin\theta,\, s\sin\theta + t\cos\theta)\,\mathrm{d}t \qquad (1)$$

where t is the direction along the line-of-sight measurement and $c(x, y)$ is the unknown distribution to be reconstructed (Fig. 2).

In a real experiment, a line-of-sight measurement $p^{k_\nu}(s, \theta)$ might be obtained by measuring the attenuation of a laser beam as it passes through the unknown distribution, i.e.,

$$p^{k_\nu}(s,\theta) = -\ln\frac{I}{I_0} = \int_{-\infty}^{+\infty} k_\nu(s\cos\theta - t\sin\theta,\, s\sin\theta + t\cos\theta)\,\mathrm{d}t \qquad (2)$$

where I is the intensity of the laser at the detector (after passing through the distribution) and $k_\nu(x, y)$ is the absorption coefficient distribution. Line integrals taken through the concentration distribution are used in this work to simulate experimental line-of-sight absorption measurements. An absorption measurement is obtained by measuring the attenuation of a laser beam and is a function of $k_\nu(x, y)$ [as described in Eq. (2)], which is in turn a function of the temperature and concentration distributions of the species under investigation. In a combustion experiment where the temperature varies, laser absorption measurements obtained at two or more frequencies are required to reconstruct concentration distributions

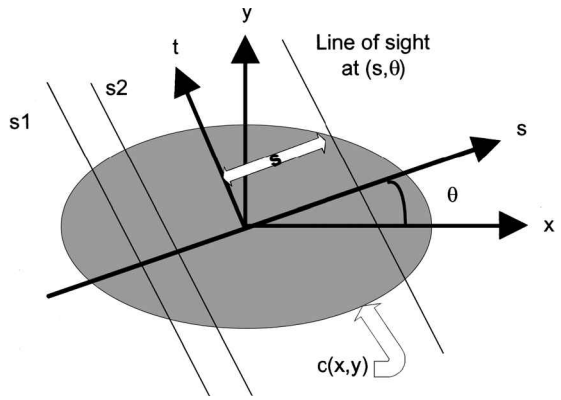

Fig. 2 Measurement geometry for the tomographic inversion problem; x and y are laboratory coordinates. At a given viewing angle θ, line-of-sight measurements are taken through lines parallel to t at given offsets ($s1$, $s2$, etc.) through the distribution $c(x, y)$ to be reconstructed.

because temperature distributions must also be determined. Further, in an actual combustion experiment it is likely that another species such as methane rather than H_2, which does absorb in the infrared, would be studied. Note, in general, that the inversion problem is ill posed because the line-of-sight measurements are taken only at a discrete set of offsets and angles.

B. Reconstruction via the TRKB Method

The TRKB method makes the inversion problem well posed by assuming that the concentration distribution to be reconstructed, $c(x, y)$, is a linear combination of basis functions $\phi_l(x, y)$, i.e.,

$$c(x_i, y_j) = \sum_{l=1}^{N_B} \alpha_l \phi_l(x_i, y_j)$$
$$i = 1, 2, \ldots, N_x, \qquad j = 1, 2, \ldots, N_y \tag{3}$$

N_B indicates the number of basis functions used in the expansion, and α_l are the basis function coefficients. The novel feature of the TRKB method is the use of K–L eigenfunctions as basis functions. The K–L eigenfunctions are chosen as a basis set for the inversion process because they optimally represent the a priori information in the training set, are easily calculated using the K–L procedure, and are capable of representing all types of distributions. Recall that a priori information is knowledge regarding the characteristics of the distributions to be reconstructed, such as the physical extent, nonnegativity, and shape of the distributions. As already mentioned, the K–L eigenfunctions form an optimal basis, which means that the fewest terms (as compared to any other basis functions) are needed to achieve a given level of accuracy in the representation of distributions in the training set. If the training set contains distributions characteristic of the distributions to be reconstructed, then only a few K–L eigenfunctions are needed as basis functions for the reconstruction. Because only a few eigenfunctions are needed to perform the reconstruction, only a small number of line-of-sight measurements is required to determine the appropriate basis function coefficients.

C. Determination of the Basis Function Coefficients

To obtain a reconstruction, it is necessary to determine the basis function coefficients in Eq. (3). The basis function coefficients are determined by formulating a least-squares problem to minimize the norm[3]

$$\| P^{\phi} \boldsymbol{\alpha} - \boldsymbol{p}^{c} \| \tag{4}$$

where P^{ϕ} is the eigenfunction projection matrix containing line integrals of the eigenfunctions, $\boldsymbol{\alpha}$ is a vector containing the unknown basis function coefficients, and $\boldsymbol{p}^{c}$ is a vector containing the line integrals of the unknown concentration distribution [see Eq. (1)]. In an actual combustion experiment, the elements of $\boldsymbol{p}^{c}$ are the line-of-sight absorption measurements, i.e., measurements of laser attenuation. Because the number of line integrals N_L is greater than the number of basis functions N_B, the least-squares problem is overdetermined, which reduces the effect of noise or random error on the determination of the unknown coefficients $\boldsymbol{\alpha}$ (Ref. 15). This overdetermined least-squares problem, which may be rank deficient/ill conditioned (see Results section), is solved using singular value decomposition.[16]

D. K–L Procedure

The K–L procedure[1,2] is a general mathematical tool that we have applied to the tomographic inversion problem. In the square jet simulations, the K–L procedure is used to identify large-scale spatial structures in a systematic manner, from which information regarding the spatiotemporal behavior of the concentration distributions in the jet may be developed. The procedure is well suited to study the square jet simulation because, as we will show, there are only a few dominant eigenfunctions or spatial structures present in the concentration distributions of the square jet. Additionally, the K–L procedure has been used previously by a number of researchers to identify spatial structures in physical flows.[1,2,17] The procedure decomposes the concentration distributions in the square jet into more important eigenfunctions, as well as less important eigenfunctions with respect to the representation of the concentration distributions, and provides quantitative measures of the relative contribution of each eigenfunction.

The K–L eigenfunctions are formed from a set of distributions called the training set. The K–L eigenfunctions are mathematically constructed to form an optimal, orthogonal basis for the representation of any distribution in the training set. In practice, the distributions in the training set can be obtained in a number of ways, including point-by-point probe sampling of the system or application of another tomographic method. In this paper, the square jet simulation provides fuel concentration distributions for the training set at various downstream locations as a series of time realizations.

Mathematically, the K–L procedure, as applied in this case, decomposes the training set of fuel concentration distributions $\{c\}$ calculated at a set of discrete time realizations (denoted by k) into a set of orthonormal eigenfunctions $\{\phi\}$ and associated time coefficients $\{a\}$:

$$c(x_i, y_j, k) = \sum_{l=1}^{N_M} a_l(k) \phi_l(x_i, y_j)$$
$$i = 1, \ldots, N_x, \qquad j = 1, \ldots, N_y, \qquad k = 1, \ldots, N_t \tag{5}$$

The K–L eigenfunctions are determined using the method of snapshots,[2,3] which states that the associated time coefficients and eigenfunctions are calculated by solving the matrix eigenvalue problem

$$DA = A\Lambda \tag{6}$$

where $D \in \boldsymbol{R}^{N_t \times N_t}$, $A \in \boldsymbol{R}^{N_t \times N_M}$, and $\Lambda \in \boldsymbol{R}^{N_M \times N_M}$; A is a matrix containing the associated time coefficients for all of the eigenfunctions; and Λ is a diagonal matrix containing the N_M eigenvalues (discussed subsequently) along the diagonal. The two-time correlation matrix D is defined by

$$D = (1/N_t) C G C^T \tag{7}$$

where $N_p (= N_x \times N_y)$ is the number of spatial points; $C \in \boldsymbol{R}^{N_t \times N_p}$ and $G \in \boldsymbol{R}^{N_p \times N_p}$; C is the training set; and G is the appropriate integration matrix, which performs a spatial integration as dictated by the continuous formulation.[3] Once A and Λ are determined by solving Eq. (6), the K–L eigenfunctions are calculated using

$$\Phi = (1/N_t) \Lambda^{-1} A^T C \tag{8}$$

where $\Phi \in \boldsymbol{R}^{N_M \times N_p}$ is a matrix containing N_M eigenfunctions.

Each eigenfunction ϕ_i has an associated eigenvalue λ_i classifying the importance or energy of that eigenfunction in the representation of distributions in the training set. Because the K–L procedure is often applied to fluid mechanical problems where the eigenvalues

measure the kinetic energy of the flow, the terminology of the eigenvalue as a measure of energy has become prevalent.[1,17] We retain the use of the eigenvalues as a measure of energy, although the eigenvalues do not correspond to the kinetic energy of the flow. The eigenfunctions are arranged in order of importance, i.e., the first eigenfunction has the largest eigenvalue, the second eigenfunction has the second largest eigenvalue, and so on. The total amount of information or energy contained in a subset of eigenfunctions is classified using normalized eigenvalues. A normalized eigenvalue $\bar{\lambda}_i$ is defined as[2]

$$\bar{\lambda}_i = \frac{\lambda_i}{\sum_{j=1}^{N_M} \lambda_j} \tag{9}$$

Further, the normalized energy in the first M eigenfunctions E_M is defined as

$$E_M = \sum_{i=1}^{M} \bar{\lambda}_i \tag{10}$$

Therefore, given a set of eigenfunctions and eigenvalues, it is possible to quantify the amount of information or energy contained in a subset of M eigenfunctions.

E. Reconstruction Methodology

Recall that the purpose of the numerical experiments is to evaluate the capability of the TRKB method to reconstruct concentration distributions from the square jet simulation at several downstream locations. The effectiveness of the K–L procedure to construct an effective basis function set for the inversion must be evaluated. Other questions must also be addressed. Is there a subset of eigenfunctions that captures the important features in the concentration distributions of the square jet simulation? How do the concentration distributions in the jet behave downstream of the jet exit? How does the measurement configuration affect the reconstruction? How does the number of eigenfunctions used in the reconstruction affect the results?

The numerical experiments consist of two processes: 1) the representation process and 2) the inversion process. The representation process relates to the formation of the K–L eigenfunctions from a training set composed of concentration distributions at a single downstream location at 80 time realizations. Because the eigenfunctions form an optimal basis set, only a subset of eigenfunctions is needed to capture the major features of the concentration distributions at a given downstream location. The inversion process uses a subset of K–L eigenfunctions as a basis set for the reconstruction of a concentration distribution at the given downstream location. Line integrals of the eigenfunctions and the concentration distribution are calculated, and a least-squares problem is posed [Eq. (4)]. The singular value decomposition is then used to solve for the basis function coefficients and determine a reconstruction. This process is shown schematically in Fig. 3. The inversion process is repeated for concentration distributions taken at different time realizations and for different arrangements of line integrals (known as measurement configurations).

IV. Results

Results obtained from performing numerical experiments on the square jet simulation data at various downstream locations are examined. The results are separated into two sections, the representation and inversion results. The representation results cover the K–L analysis of concentration distributions at downstream locations near the jet exit ($5dx$), far from the jet exit ($105dx$), and an intermediate distance from the jet exit ($65dx$). The inversion results focus on downstream locations farther from the jet exit, where the flow is more complex and tomographic inversion is more challenging. Inversion results are shown for positions $65dx$, $85dx$, and $105dx$.

A. TRKB Inversion: Representation Results

The first K–L eigenfunctions, formed by performing the K–L procedure on sets of concentration distributions for 80 time realizations at the downstream locations $5dx$, $65dx$, and $105dx$ are shown in Fig. 4. The normalized eigenvalue spectra for all three downstream locations are shown in Fig. 5.

At downstream location $5dx$, the first eigenfunction has a square top-hat shape, whereas at positions $65dx$ and, especially, $105dx$, the first eigenfunction has rounded features and ridges extending away from the jet axis. Because the first eigenfunction has the largest eigenvalue, it can be considered to be the distribution most correlated with all of the concentration distributions at the given downstream location. Therefore, the first eigenfunction traces the downstream development of the fuel concentration in the flow from a uniform concentration at the jet exit to a more diffuse and complex distribution farther downstream.

The normalized eigenvalue spectra show the relative importance of each eigenfunction in the representation of distributions in the training set. The normalized eigenvalue spectra show that the energy or information associated with the first few eigenfunctions decreases with downstream location. This can be seen quantitatively by examining E_M, defined in Eq. (10), for downstream locations $5dx$, $65dx$, and $105dx$ (Table 1). Because the energy in the first few eigenfunctions decreases with downstream location, the energy in the other eigenfunctions must increase. Therefore, to represent the

Table 1 Comparison of the energy contained in a subset of K–L eigenfunctions at downstream locations $5dx$, $65dx$, and $105dx$

E_M[a]	$5dx$, %	$65dx$, %	$105dx$, %
E_1	>99.9	93.1	80.5
E_6	>99.9	98.2	93.4
E_{10}	>99.9	98.9	96.1

[a]Defined in Eq. (10).

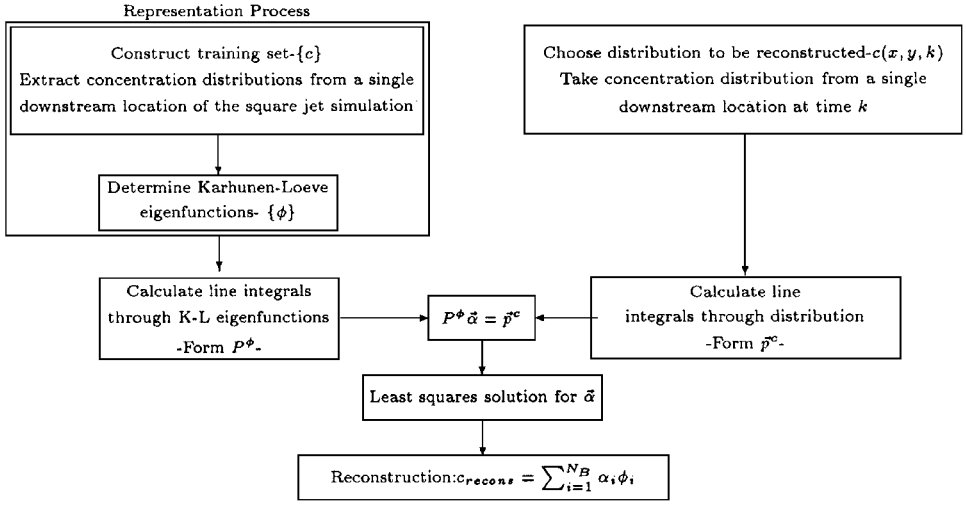

Fig. 3 Flowchart of the TRKB reconstruction process, including the representation process (shown in the box in the upper-left-hand corner) and the inversion process (everything outside the box in the upper-left-hand corner).

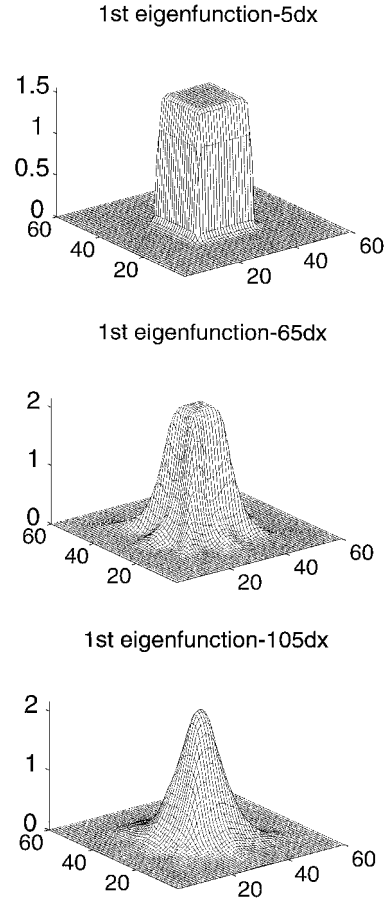

Fig. 4 First K–L eigenfunctions for downstream locations 5*dx*, 65*dx*, and 105*dx*.

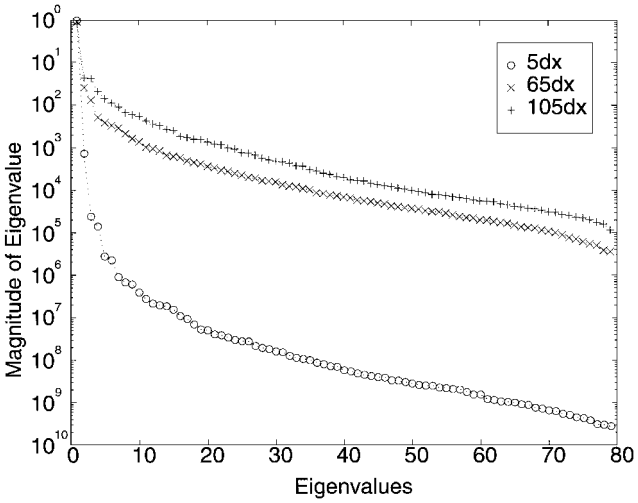

Fig. 5 Normalized eigenvalue spectra for downstream locations 5*dx*, 65*dx*, and 105*dx*.

significant features in the flow, more eigenfunctions must be used in the representation as one proceeds farther downstream.

Another way to examine the downstream development of the flow, as well as the representational capabilities of the K–L eigenfunctions, is to consider the representation of concentration distributions in the training set. The best representation of a concentration distribution $c(x, y, t_k)$ by a subset containing M K–L eigenfunctions is

$$c(x, y, t_k) \cong \hat{c}(x, y, t_k) = \sum_{i=1}^{M} a_i(t_k)\phi_i(x, y) \tag{11}$$

where $\hat{c}(x, y, t_k)$ is the best representation of $c(x, y, t_k)$ given only the first M eigenfunctions. The best representation of the concentration distribution is simply the sum of the first M eigenfunctions and their associated time coefficients a_i as determined by the K–L procedure.[3] The representation $\hat{c}(x, y, t_k)$ is called the best representation of $c(x, y, t_k)$ because it minimizes the difference between $\hat{c}$ and c given the first M eigenfunctions. Mathematically stated, the best representation minimizes the norm, $\|c - \hat{c}\|$, given M eigenfunctions.[3]

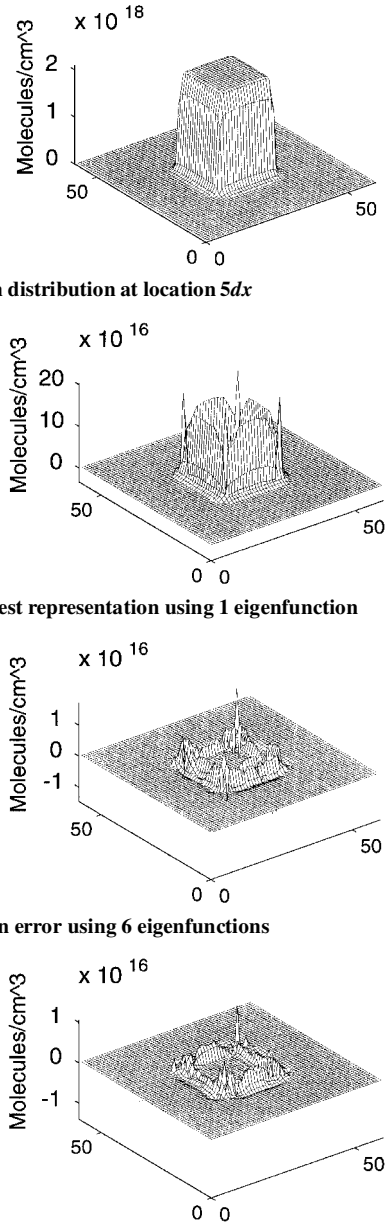

Fig. 6 Representation of a concentration distribution at downstream location 5*dx*.

The representation of a concentration distribution at $5dx$ using 1, 6, and 10 eigenfunctions is shown in Fig. 6. Similarly, representation results for downstream locations $65dx$ and $105dx$ are shown in Figs. 7 and 8, respectively. The representational capability of a subset of eigenfunctions is demonstrated by the relatively small (in comparison with the magnitude of the concentration distributions being represented) representation errors present. Because the flow develops downstream, at $5dx$ the concentration distribution is more effectively represented than at $65dx$ and $105dx$ using the same number of eigenfunctions. The representation results are quantified using two error measures.[18]

1) Normalized rms measure

$$\text{rms} = \frac{\|c(x_i, y_j) - \hat{c}(x_i, y_j)\|_F}{\|c(x_i, y_j) - \bar{c}\|_F} \tag{12}$$

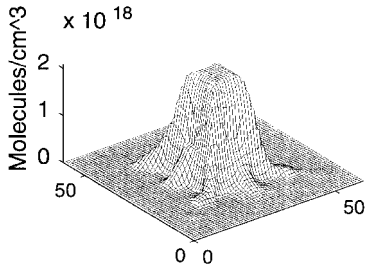

Concentration distribution at location 65*dx*

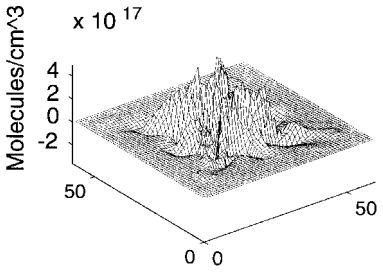

Error in the best representation using 1 eigenfunction

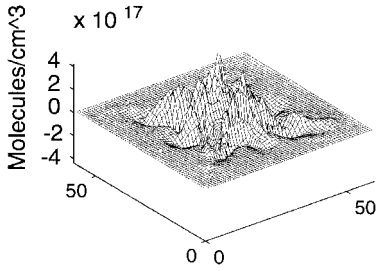

Representation error using 6 eigenfunctions

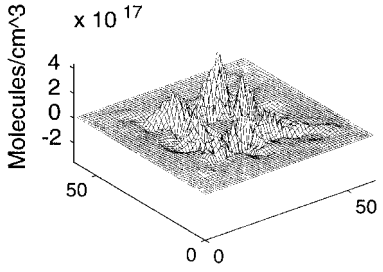

Representation error using 10 eigenfunctions

Fig. 7 Representation of a concentration distribution at downstream location 65*dx*.

where

$$\bar{c} = \sum_{i=1}^{N_x} \sum_{j=1}^{N_y} \frac{c(x_i, y_j)}{N_x N_y}$$

is the average value of the distribution and $\| \cdot \|_F$ denotes the Frobenius norm. Recall that the Frobenius norm of a matrix is the square root of the sum of the squared elements of the matrix.

2) Normalized absolute measure

$$\text{abs} = \left[\sum_{i=1}^{N_x} \sum_{j=1}^{N_y} |c(x_i, y_j) - \hat{c}(x_i, y_j)| \right] \Bigg/ \left[\sum_{i=1}^{N_x} \sum_{j=1}^{N_y} |c(x_i, y_j)| \right] \tag{13}$$

The decrease in the representation error as the number of eigenfunctions is increased can be further demonstrated by using the normalized rms and abs error measures. Table 2 shows that at each downstream location the representation error decreases as the number of eigenfunctions is increased.

The application of the K–L procedure to the square jet simulation has shown the development of the square jet with downstream position. It has also been shown that it is necessary to use more eigenfunctions to represent the more complex features present at farther downstream locations. Because these eigenfunctions serve as basis functions for the reconstruction, the need to use a greater number of eigenfunctions directly affects the inversion process (see Inversion Results).

Table 2 Results of representing a concentration distribution at downstream locations 65*dx*, 85*dx*, and 105*dx*

No. of eigenfunctions:	1	6	10
RMS 5*dx*	0.0375	0.00179	0.00119
ABS 5*dx*	0.0289	0.00124	8.06e-4
RMS 65*dx*	0.163	0.130	0.108
ABS 65*dx*	0.182	0.147	0.114
RMS 105*dx*	0.635	0.311	0.223
ABS 105*dx*	0.690	0.387	0.269

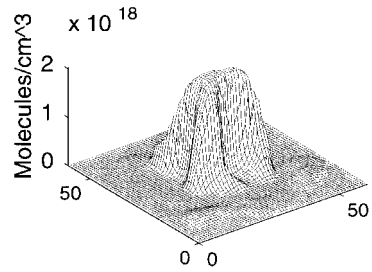

Concentration distribution at location 105*dx*

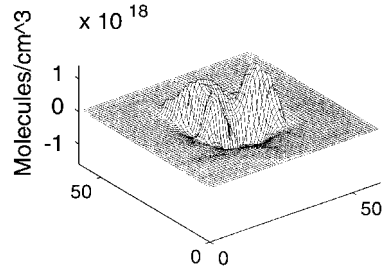

Error in the best representation using 1 eigenfunction

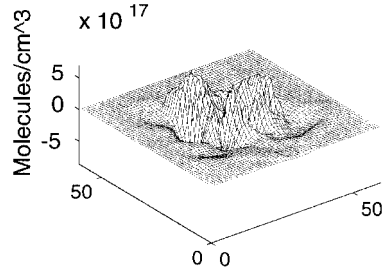

Representation error using 6 eigenfunctions

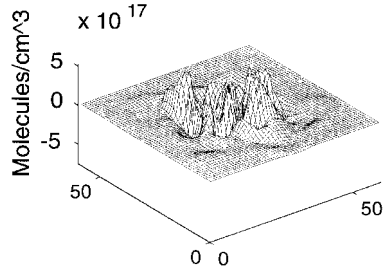

Representation error using 10 eigenfunctions

Fig. 8 Representation of a concentration distribution at downstream location 105*dx*.

B. TRKB Inversion: Inversion Results

The reconstruction of 80 concentration distributions at three downstream locations, 65*dx*, 85*dx*, and 105*dx*, was performed using numerically simulated line-of-sight measurements (line integrals). Accurate reconstructions capturing the major features of the

flow were obtained using only 28 line integrals obtained at four viewing angles (0, 45, 90, and 135 deg). Reconstructions using 42 line integrals obtained at six viewing angles (0, 45, 63, 90, 135, and 153 deg) were also performed for comparison. In general, the number of eigenfunctions used in the reconstruction and the condition number of the eigenfunction projection matrix were found to affect the reconstruction accuracy.

Errors resulting from the reconstruction of concentration distributions can be classified into three types: reconstruction errors, representation errors, and retrieval errors (Fig. 9). The difference between the concentration distribution to be reconstructed, c, and the best representation $\hat{c}$ using M eigenfunctions is called the representation error. The size of the representation error is determined by the number of eigenfunctions used in the best representation. As the number of eigenfunctions increases, the best representation more closely represents the concentration distribution, and the representation error decreases. Ultimately, the best representation $\hat{c}$ is equivalent to the concentration distribution c if all of the basis functions N_B are used in the representation. The difference between the reconstructed distribution c_{recons} using M eigenfunctions and the concentration distribution c is called the reconstruction error. The difference between the best representation and the reconstructed distribution is called the retrieval error. The size of the retrieval and reconstruction error is determined by the accuracy of the reconstructions produced by the inversion process. The minimum reconstruction error using M eigenfunctions occurs when the reconstructed distribution equals the best representation and the retrieval error goes to zero. Reconstruction, representation, and retrieval errors can all be quantified using the error measures described earlier.

The reconstruction of a concentration distribution at the downstream location $65dx$ is shown in Fig. 10. This reconstruction uses only 11 eigenfunctions and 28 line integrals over four viewing angles. The normalized rms and absolute measures for the reconstruction error are 0.122 and 0.137, respectively, for the reconstruction shown in Fig. 10. The normalized rms and absolute measures for the retrieval error are 0.064 and 0.058, respectively, for the same reconstruction. The normalized rms and absolute measures for the representation error are 0.104 and 0.116, respectively, for the same reconstruction. The error in the reconstruction (in Fig. 10) is predominantly small except for a number of sharp peaks corresponding to regions of high gradients in the original distribution. Rather than show all of the reconstruction results performed in this study, the reconstruction in Fig. 10 is provided as a sample result that is typical of those obtained using the TRKB method, and henceforth, a summary of the reconstruction results is presented.

The results of reconstructing all 80 concentration distributions at $65dx$ using only 28 line integrals are shown in Table 3. The normalized rms and absolute measures shown in Table 3 are mean values obtained by averaging the reconstruction results of all 80 distributions. At location $65dx$, 11 eigenfunctions correspond to an energy of 99% ($E_{11} = 99\%$). The number of eigenfunctions required to achieve an energy of 99% at location $85dx$ is 19. The results of reconstructing all 80 concentration distributions at location $85dx$ using 19 eigenfunctions and 28 line integrals are shown in Table 3. Similarly, the results of reconstructing all 80 concentration distributions at location $105dx$ using 24 eigenfunctions (99% energy) are shown in Table 3. It is seen that, although the reconstruction results worsen as one progresses downstream, the reconstruction results are, in general, accurate using only 28 measurements.

The results of reconstructing all 80 concentration distributions at $65dx$, $85dx$, and $105dx$ using 42 line integrals (seven measurements at six angles) are shown in Table 4. The values listed in Table 4 are obtained in the same manner as in Table 3 except that 42 line integrals were used rather than 28 line integrals; 11 eigenfunctions, 19 eigenfunctions, and 24 eigenfunctions were used to perform reconstructions at locations $65dx$, $85dx$, and $105dx$, respectively. Because 42 line integrals provide more information regarding the distribution to be reconstructed than 28 line integrals, the reconstruction results using 42 line integrals are more accurate. (Condition numbers are lower for 42 measurements; see subsequent discussion.)

Table 3 Results of reconstructing 80 concentration distributions using 28 line integrals (seven measurements at four viewing angles: 0, 45, 90, and 135 deg)

Value	$65dx$	$85dx$	$105dx$
		Reconstruction error	
RMS	0.130	0.165	0.284
ABS	0.146	0.195	0.330
		Retrieval error	
RMS	0.075	0.127	0.261
ABS	0.075	0.146	0.300
		Representation error	
RMS	0.105	0.105	0.109
ABS	0.122	0.128	0.137
		Condition number	
$\kappa(P^{\phi})$	7.5	12	42
		No. of eigenfunctions	
	11	19	24

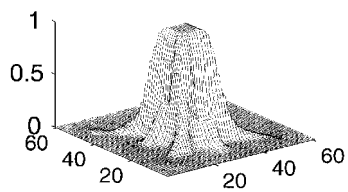

Concentration distribution normalized by maximum concentration at $65dx$

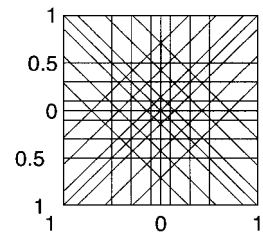

Measurement configuration used to perform the reconstruction

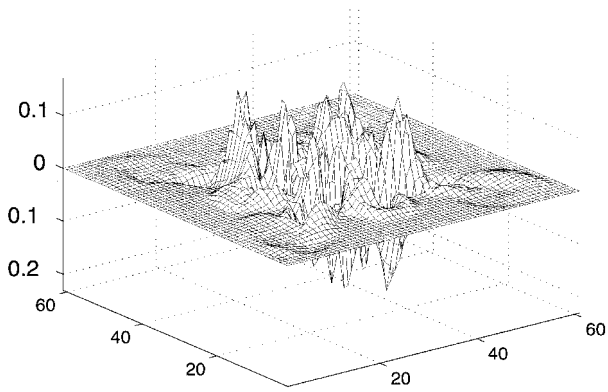

Reconstruction error

Fig. 10 Reconstruction of a concentration distribution at downstream location $65dx$ using 11 eigenfunctions.

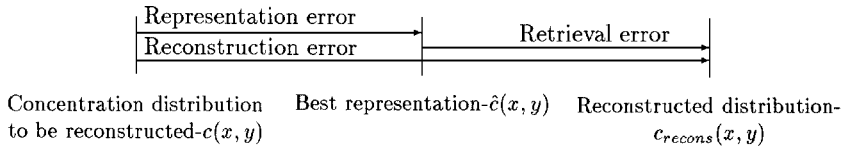

Fig. 9 Reconstruction errors.

Table 4 Results of reconstructing 80 concentration distributions using 42 line integrals (seven measurements at six viewing angles: 0, 45, 63, 90, 135, and 153 deg)

Value	$65dx$	$85dx$	$105dx$
		Reconstruction error	
RMS	0.120	0.128	0.154
ABS	0.136	0.152	0.182
		Retrieval error	
RMS	0.057	0.074	0.108
ABS	0.058	0.084	0.128
		Representation error	
RMS	0.105	0.105	0.109
ABS	0.122	0.128	0.137
		Condition number	
$\kappa(P^{\phi})$	5.1	6.3	11
		No. of eigenfunctions	
	11	19	24

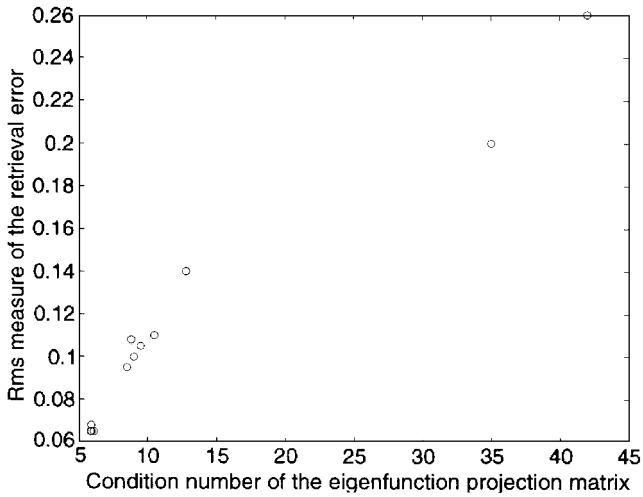

Fig. 11 Comparison of condition number of the eigenfunction projection matrix and the mean normalized rms measure of the retrieval error for reconstructing 80 distributions at location $105dx$.

In general, the reconstruction accuracy at a given downstream location depends on the measurement configuration (number and arrangement of measurement lines of sight) and the number of eigenfunctions used in the reconstruction.

Intuitively, some measurement configurations will produce more accurate reconstructions than others. Quantitatively, the effectiveness of a measurement configuration can be measured using the condition number of the eigenfunction projection matrix P^{ϕ} (Ref. 3). The condition number $\kappa(P^{\phi})$ is defined as

$$\kappa(P^{\phi}) = \sigma_1/\sigma_n \tag{14}$$

where σ_1 and σ_n are the largest and smallest singular values of P^{ϕ}, respectively, and may be obtained from the singular value decomposition of P^{ϕ}. If the condition number is large [$\mathcal{O}(10^2)$], the eigenfunction projection matrix is ill conditioned, and large errors may result when calculating the reconstruction. Conversely, if the condition number is small [$\mathcal{O}(10^1)$], then the eigenfunction projection matrix is well conditioned, and small errors result when calculating the reconstruction. The effect of $\kappa(P^{\phi})$ on the mean normalized rms measure of the retrieval error is shown in Fig. 11, where the reconstruction of 80 concentration distributions at location $105dx$ is shown. $\kappa(P^{\phi})$ is varied by choosing different measurement configurations. Note that, in Fig. 11, 12 different measurement configurations are used, and all reconstructions used 24 eigenfunctions. For each $\kappa(P^{\phi})$, all 80 concentration distributions at $105dx$ are reconstructed and the mean normalized rms measure of the retrieval error is calculated. Examination of Fig. 11 shows that, as $\kappa(P^{\phi})$ decreases, the accuracy of the reconstruction, as measured by the mean normalized rms measure, increases. Smaller condition numbers are the reason for the lower reconstruction and retrieval errors using 42 line integrals (Table 4) instead of 28 line integrals (Table 3).

The reconstruction accuracy is also affected by the number of eigenfunctions used. Earlier in this section, it was demonstrated that, as the flow develops downstream and becomes more complex, the number of eigenfunctions needed to represent the major features of the flow increases. Therefore, reconstructions performed farther downstream require more eigenfunctions for the same representation accuracy. Superficially, the use of as many eigenfunctions as possible to perform the reconstructions poses an attractive option because the more eigenfunctions that are included, the greater the number of flow features that are captured. This idea is limited because the higher (60th, 70th, ...) eigenfunctions contain substantially less energy than the lower (1st, 2nd, ...) eigenfunctions (see Fig. 5), so that the relative contribution of each of the higher eigenfunctions is considerably smaller than that of the lower eigenfunctions. Also, given a set of line-of-sight measurements to perform a reconstruction, as the number of eigenfunctions increases, the condition number of the eigenfunction projection matrix rises and the retrieval error increases. This is the reason for the increased error at location $105dx$ as compared with $65dx$ in Table 3. In both cases, the same set of line-of-sight measurements is used, and the representation error at both locations is the same. The difference is that, at $65dx$, 11 eigenfunctions are used, and at $105dx$, 24 eigenfunctions are used. This results in a higher condition number at location $105dx$, $\kappa(P^{\phi}) = 42$, than at $65dx$, $\kappa(P^{\phi}) = 7.5$, producing higher errors in the reconstruction at $105dx$.

V. Summary and Conclusions

Numerical experiments using the TRKB method have successfully reconstructed fuel concentration distributions at various downstream locations in an unsteady, reacting flow obtained from a numerical simulation of a turbulent reacting square jet. Training sets were constructed using concentration distributions at given downstream locations. The K–L procedure was applied to the training sets to produce sets of K–L eigenfunctions, which serve as the basis functions for the tomographic inversion. Because the K–L eigenfunctions form an optimal basis, a small subset of K–L eigenfunctions captures the significant features of the concentration distributions. As the scalar fields developed downstream, it was necessary to use more eigenfunctions (than at the jet exit) to represent their increasingly complex structure. With a subset of eigenfunctions as basis functions, accurate reconstructions of concentration distributions were obtained with only 28 and 42 line integrals.

The training set, which contained fuel concentration distributions from the reacting turbulent square jet simulation, was larger (80 members) and more characteristic of unsteady combustion situations than any previous work with the TRKB method. To perform accurate reconstructions requiring only a few measurements, it was necessary that the K–L eigenfunctions compactly represent the significant features in the distributions. Because of their optimal nature, the K–L eigenfunctions effectively captured the spatiotemporal behavior of the distributions with only a few members. A subset of only 24 eigenfunctions was required to capture the prominent features at location $105dx$, whereas many fewer were required closer to the jet exit.

Several generalizations regarding the TRKB method can be made from the results. The condition number of the eigenfunction projection matrix was found to measure the effect of a given measurement configuration on the accuracy of the reconstruction. The number of eigenfunctions used in the reconstruction was determined to be an important consideration in the reconstruction process. If too many eigenfunctions are used for a fixed number of measurements, then the accuracy of the reconstruction is compromised (retrieval error), but if too few eigenfunctions are used, then the distribution to be reconstructed is inadequately represented (representation error). To determine the proper number of eigenfunctions, one must first choose a subset of eigenfunctions that provides a satisfactory representation of the flow. Second, the measurement configuration and the number of lines of sight must be determined such that the eigenfunction projection matrix has a small condition number. Given that these two criteria are satisfied, accurate reconstruction can be performed. Fortunately, these two criteria can be satisfied prior to any reconstruction, given that a training set has been obtained. In addition, the numerical experiments can be used to design a combustion

experiment providing a framework for the experimental setup. For example, the measurement configuration resulting in the smallest condition number can guide the arrangement and number of absorption measurements in the experiment.

Although the TRKB method successfully reconstructed concentration distributions in the numerical experiments, the practical implementation of the TRKB method as a combustion diagnostic tool involves issues outside of the scope of this paper. These issues include the construction of a training set in cases where numerical simulation is not appropriate, modeling the path of the line-of-sight measurements, the effect of experimental error on the reconstruction accuracy, and problems associated with optical access. These issues have been examined in detail elsewhere for a steady, nonreacting flow. In a reacting flow, reconstruction of concentration and temperature distributions requires absorption measurements performed at two or more frequencies. If the flow is unsteady, it is also necessary to obtain the absorption measurements quickly enough to capture the transient features. These issues associated with the experimental implementation of the TRKB method on unsteady reacting flows are currently being investigated.

Acknowledgments

This work is funded by the U.S. Army under Army Research Office Grant DAAL03-92-G-0113. Alexander Hinz was supported by the German Academic Exchange Service and a Lewis fellowship. The authors would like to gratefully acknowledge the assistance and cooperation of F. F. Grinstein and K. Kailasanath.

References

[1]Berkooz, G., Holmes, P., and Lumley, J. L., "The Proper Orthogonal Decomposition in the Analysis of Turbulent Flows," *Annual Review of Fluid Mechanics*, Vol. 25, 1992, pp. 539–575.

[2]Sirovich, L., and Everson, R., "Management and Analysis of Large Scientific Datasets," *International Journal of Supercomputer Applications*, Vol. 6, No. 1, 1992, pp. 50–68.

[3]Torniainen, E. D., and Gouldin, F. C., "Tomographic Reconstruction of 2-D Distributions Using a Karhunen–Loève Basis," *Applied Optics* (submitted for publication).

[4]Torniainen, E. D., Lam, K. W., Chojnacki, A. M., Gouldin, F. C., and Wolga, G. J., "Tomographic Reconstruction of Absorption Coefficient Distributions from a Limited Number of Laser Absorption Measurements," *1995 Fall Technical Meeting of the Eastern States Section of the Combustion Institute* (Worcester, MA), Combustion Inst., Pittsburgh, PA, 1995, pp. 63–66.

[5]Torniainen, E. D., and Gouldin, F. C., "Tomographic Reconstruction of 2-D Methane Concentration Distributions from a Limited Set of Infrared Absorption Data," *Combustion Science Technology*, Vol. 131, No. 1–6, 1998, p. 85.

[6]Chojnacki, A. M., Sarma, A., Wolga, G. J., Torniainen, E. D., and Gouldin, F. C., "Infrared Tomographic Inversion for Combustion and Incineration," *Combustion Science Technology*, Vol. 116/117, 1996, pp. 583–606.

[7]Grinstein, F. F., and Kailasanath, K., "Three-Dimensional Numerical Simulations of Unsteady Reactive Square Jets," *Combustion and Flame*, Vol. 100, No. 1/2, 1995, pp. 2–10.

[8]Best, P. E., Chien, P. L., Carangelo, R. M., Solomon, P. R., Danchak, M., and Ilovici, I., "Tomographic Reconstruction of FT-IR Emission and Transmission Spectra in a Sooting Laminar Diffusion Flame: Species Concentrations and Temperatures," *Combustion and Flame*, Vol. 85, No. 3/4, 1991, pp. 309–318.

[9]Emmerman, P. J., Goulard, R., Santoro, R. J., and Semerjian, H. G., "Multiangular Absorption Diagnostics of an Argon–Methane Jet," *Journal of Energy*, Vol. 4, No. 2, 1980, pp. 70–77.

[10]Hughey, B. J., and Santavicca, D. A., "A Comparison of Techniques for Reconstructing Axisymmetric Reacting Flow Fields from Absorption Measurements," *Combustion Science Technology*, Vol. 29, No. 3–6, 1982, pp. 167–190.

[11]Ray, S. R., and Semerjian, H. G., "Laser Tomography for Simultaneous Concentration and Temperature Measurements is Reacting Flows," *Combustion Diagnostics by Nonintrusive Methods*, edited by T. D. McCay and J. A. Roux, Vol. 92, Progress in Astronautics and Aeronautics, AIAA, New York, 1982, pp. 300–324.

[12]Ravichandran, M., and Gouldin, F. C., "Reconstruction of Smooth Distributions from a Limited Number of Projections," *Applied Optics*, Vol. 27, No. 19, 1988, pp. 4084–4097.

[13]Kak, A. C., *Principles of Computerized Tomographic Imaging*, IEEE Press, New York, 1988, pp. 49–169.

[14]Lewitt, R. M., "Reconstruction Algorithms: Transform Methods," *Proceedings of the IEEE*, Vol. 71, No. 3, 1983, pp. 390–408.

[15]Björck, A., *Numerical Methods for Least Squares Problems*, Society for Industrial and Applied Mathematics, Philadelphia, PA, 1996, p. 1.

[16]Golub, G. H., and Van Loan, C. F., *Matrix Computations*, Johns Hopkins Univ. Press, Baltimore, MD, 1985, pp. 70–75.

[17]Sirovich, L., Ball, K. S., and Keefe, L. R., "Plane Waves and Structures in Turbulent Channel Flow," *Physics of Fluids A*, Vol. 2, No. 12, 1990, pp. 2217–2226.

[18]Verhoeven, D., "Limited-Data Computed Tomography Algorithms for the Physical Sciences," *Applied Optics*, Vol. 32, No. 20, 1993, pp. 3736–3754.

G. Laufer
Associate Editor